AIAA 2011-5104

A Range of Motion Study and Human-Suit Correlation Analysis Supporting the Morphing Spacesuit Concept

Heather N. Bradshaw[1] and Dr. David L. Akin[2]
Space Systems Laboratory, University of Maryland, College Park, MD 20740

and

Dr. J. Sean Humbert[3]
Autonomous Vehicle Laboratory, University of Maryland, College Park, MD 20740

This paper describes continuing research supporting the Morphing Upper Torso spacesuit design, which uses robotic augmentation of a rear-entry pressure suit to adjust torso dimensions. This concept has the potential to provide easier ingress/egress of the suit, increased mobility when pressurized, and reduced astronaut workload during extravehicular operations. In previous work, the forward and inverse kinematics for the system have been solved, two static models have been built, and data from a range-of-motion (ROM) study has been collected using a Vicon motion capture system. During the ROM study, test subjects wore simulated shoulder scye bearings as they performed selected tasks, with the intent to measure human motion in relation to scye bearing motion. The research presented in this paper describes the data analysis and results of the ROM study. This includes an investigation of the neutral pose observed for the scye bearings when the subject is standing at rest in Earth gravity, with the arms hanging at the subject's sides, as well as an analysis of the angular range-of-motion observed for the right scye bearing during selected tasks. This paper also presents the development of a heuristic relationship between the motion of the right arm and right scye bearing. The results of this correlation model, applicable to a limited but useful region of motion, provide a mapping between a known arm pose and the desired scye bearing pose needed to facilitate the astronaut's motion with minimum suit forces. This research is a critical next step towards the development and testing of a fully functional Morphing Upper Torso spacesuit prototype.

Nomenclature

α_{arm}	=	alpha angle of rotation of arm, measured from negative z axis in base frame
α_{SB}	=	angle of rotation of scye bearing about its local x axis
c	=	cosine
DOF	=	degrees of freedom
EMU	=	extravehicular mobility unit
EVA	=	extravehicular activity
γ_{arm}	=	angle of rotation of arm, measured from positive x axis in base frame
γ_{SB}	=	angle of rotation of scye bearing about its local z axis
LS	=	left scye bearing
MATLAB	=	Matrix Laboratory (Mathworks, Inc.)
MUT	=	morphing upper torso

[1] Graduate Researcher, Department of Aerospace Engineering, 382 Technology Drive, University of Maryland, College Park, MD 20742, Student Member.
[2] Professor, Department of Aerospace Engineering, 382 Technology Drive, University of Maryland, College Park, MD 20742, Senior Member.
[3] Professor, Department of Aerospace Engineering, 3182 Martin Hall, University of Maryland, College Park, MD 20742, Member.

R = rotation matrix
R^2 = coefficient of determination
ROM = range-of-motion
RS = right scye bearing
RSE = vector from deltoid marker to elbow marker
s = sine
SB = scye bearing
svd = singular value decomposition function
$x_{deltoid}$ = x coordinate of deltoid marker
x_{SB} = x coordinate of scye bearing center
$X_{SB,L}$ = local X axis of left scye bearing
$X_{SB,R}$ = local X axis of right scye bearing
Xu = unit vector along local X axis of right scye bearing
$y_{deltoid}$ = y coordinate of deltoid marker
y_{SB} = y coordinate of scye bearing center
$Y_{SB,L}$ = local Y axis of left scye bearing
$Y_{SB,R}$ = local Y axis of right scye bearing
Yu = unit vector along local Y axis of right scye bearing
$z_{deltoid}$ = z coordinate of deltoid marker
z_{SB} = z coordinate of scye bearing center
$Z_{SB,L}$ = local Z axis of left scye bearing
$Z_{SB,R}$ = local Z axis of right scye bearing
Zu = unit vector along local Z axis of right scye bearing

I. Introduction

MOBILITY is one of the greatest challenges in spacesuit design. It requires strength and stamina to move while wearing a spacesuit; the pressurized fabric significantly increases the amount of joint torque that must be supplied by the human in order to move his/her limbs.[1] Improving the pressurized mobility of the suit would be a major advancement in the field of spacesuit design, and a necessary step in developing the next generation of suits that will enable humans to explore the Moon, Mars, and beyond.

One of the most effective ways to improve pressurized mobility is to have a conformal suit with a close fit to the astronaut's anthropometric dimensions.[2] Because of this, during the Apollo era, suits were custom-fit to each astronaut prior to the mission. However, due to changes in body shape in a reduced gravity environment, suits that may be a perfect fit on Earth, might not be a perfect fit in space.[3] Also, while having a very close-fitting suit is desired for pressurized mobility, it causes difficulty in ingress/egress of the suit. Because of these two conflicting requirements – close fit for pressurized mobility and loose fit for ingress/egress – most suit designs offer a compromise between the two. It would be highly desirable to have a suit design that enables both.

One potential solution for this problem is a design concept for a robotically augmented suit, called the Morphing Upper Torso (MUT), which would use mechanical actuation to provide five degrees of freedom (dof) at each of the four torso bearings (shoulders, helmet, and waist) of a pressurized suit. (The sixth dof is provided by the bearing nature of the joints.) Work on the MUT concept is currently underway at the Space Systems Laboratory at the University of Maryland. This design has the potential to provide greatly enhanced mobility at each joint. To accomplish this, each torso bearing would be attached via parallel prismatic linkages to a fixed back hatch of a rear-entry suit, in addition to being attached to the other torso bearings, thereby forming a system of interconnected parallel manipulators.[4] The arrangement of prismatic linkages is shown in Figure 1. As the astronaut moves, the telescoping robotic linkages would expand or contract, causing the shape of the upper torso to change, or morph, with the astronaut's motions. Implementing a system of interconnected parallel manipulators on a suit torso is a novel application of the technology, and the kinematics for such a system were not initially known; however, previous work has since established the forward and inverse kinematics of the MUT design. Functionality of this concept has been investigated analytically, and from this work, the concept has been demonstrated to be theoretically feasible.[2] In addition, half and full scale static models have been developed.[3] An image of the half scale model is shown in Figure 2.

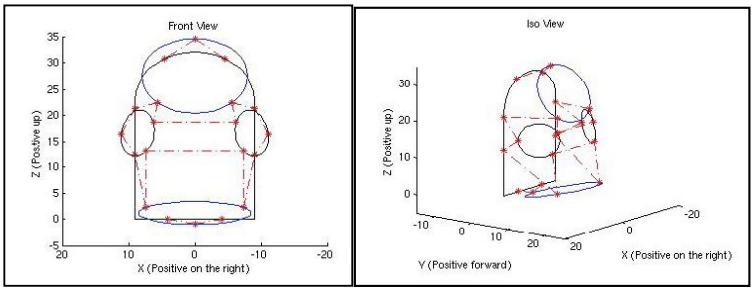

(a) **(b)**

Figure 1. (a) Front view and (b) isometric view of MUT linkage system.[3]

Figure 2. Side view of half-scale static model of MUT, lying down (waist bearing on left).[3]

The next step in the development of the MUT concept is to characterize the desired orientation of the shoulder scye bearings in relation to human arm orientation. To achieve this, a range-of-motion (ROM) study was conducted using a Vicon motion capture system in which subjects wore simulated scye bearings and performed selected motion tasks in order to observe the behavior of the scye bearings in relation to arm pose. The results of this study include an analysis of the observed neutral pose of the scye bearings, as well as identification of the angular range of motion of the right scye bearing, and the development of heuristic models which serve as a mapping between a known pose of the right arm and a corresponding desired pose of the right scye bearing applicable to a specified region.

II. Methodology

During this study, a Vicon motion capture system was used to record position data of retro-reflective markers placed on the subject. Prior to conducting this study, a simulation suit was developed, simulated scye bearings were produced, and approval was obtained for human testing. During the testing, subjects performed several motion tasks intended to move the scye bearings through their full range of motion.

A. Vicon Motion Capture System

In this study, a Vicon iQ 2.5 motion capture system was used to record the real-time position of retro-reflective markers placed on the subject. The experimental setup included eight Vicon cameras, which surrounded a subject standing in the test volume, as shown in Figure 3. The strobing cameras detected the position of the markers in Cartesian coordinates relative to a base reference frame located on the floor, in the center of the room. The data sampling rate used for this study was 350 Hz. In the data capture process, if at least two cameras detected the same marker, the system used triangulation of the intersecting light rays to determine the position of that marker in three dimensions.[5] This position data was later used to calculate the Euler angles of the scye bearings, and the orientation of the upper arm segment.

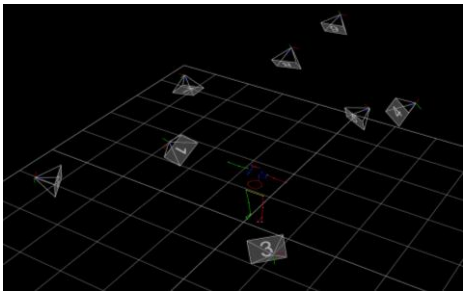

Figure 3. Subject as seen by Vicon system, surrounded by motion-capture cameras.

It is useful to note that, if the Morphing Upper Torso were to be implemented as a future spacesuit design, one would need a system of measuring body angles that is portable, and preferably would fit inside the suit. Research in areas such as smart fabrics may be able to facilitate this. For example, research is currently underway to sense foot motion, joint angles, and foot posture using conductive polymer sensors.[6] The conductive polymer technology could potentially be adapted for use on other parts of the body of interest to the morphing upper torso research (e.g., shoulders, torso, and arms). Also, more directly applicable to arm angle measurement in a spacesuit, a system is being developed at the Space Systems Laboratory of the University of Maryland which offers a portable, non-intrusive means of measuring finger bend angles as well as the attitude of the human arm; the current prototype of this system uses ten piezo-resistive bend sensors, a micro-controller, and three MEMS IMU'S (with nine dof each) located along the arm and hand.[7] Such systems would be very useful for providing the real-time body measurements needed for a dynamically adaptive suit. In the interim, the Vicon system is invaluable in performing this function during the development phase of the MUT concept.

B. Marker Placement

The requirement that at least two of the cameras must see a given marker at all times guided the decisions made with respect to marker placement on the simulation suit. For example, rather than attaching the markers to the flat surface of the simulated scye bearings, the retro-reflective markers were attached to the edge of the simulated bearings, to enable maximum camera visibility, as shown in Figure 4. If the markers had been located on the flat surface, then the planar side of the bearing (the one with markers) would likely to be angled away from at least half the cameras at any given time, reducing the chances of the marker being found. Therefore, the edges of the bearings were chosen as the optimal location.

Figure 4. Example of foamcore scye bearing simulator.

In addition to placement, consideration was given to the number of markers each scye bearing should have. At least three points are needed to define a plane, such as a shoulder bearing. For robustness, at least five markers were used on each scye bearing, with six markers used on the right scye bearing so that one could differentiate the left from the right bearing.

In addition to the scye bearings, a simulated waist bearing was also implemented, to provide a reference that would aid in visualizing the human form. For the simulated waist bearing, eight markers were used to ensure that at least three would be found at a given instant in time. A higher number of markers were used for the waist bearing because of the likelihood that one or more of the markers may be temporarily occluded from the cameras by movement of the arms.

Several markers were also placed on anthropometric landmarks of the body, which would offer a consistent marking location proportional to each person. A diagram of the selected fiducial locations is shown in Figure 5. Of particular interest are the markers on the deltoid and elbow, as these were used to calculate the orientation of the upper arm segment. The deltoid marker was placed one finger-width below the hinge point of the shoulder joint when the arm was raised at full abduction. The intent was to place the marker as close to the top of the shoulder joint as possible, while still located on a "rigid" part of the arm. Similarly, the elbow marker was located one finger-width above the hinge point of that joint, approximately along the line of non-extension. A list of the other body marker locations is provided below:

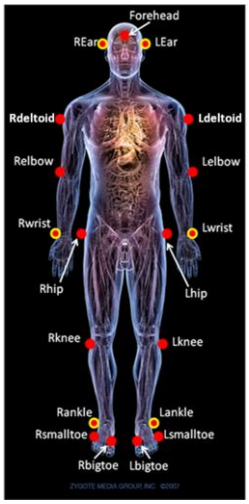

Figure 5. Location of retro-reflective markers on subject. *Image of human body from Ref. 8.*

- Forehead: attached to a headband, centered above the nose
- Ear: attached to a headband, directly above the tips of left and right ears
- Wrist: triquetrum bone
- Hip: top of femur
- Knee: top of fibula
- Ankle: medial maleolus bone
- Big toe: the first M-P joint
- Little toe: the fifth M-P joint

C. Simulation Suit

In order to conduct experiments using the Vicon system, it was necessary to first develop a simulation suit to be worn during testing. The purpose of the garment was to provide a medium for attaching the retro-reflective markers. The markers needed to be securely fixed to the subject in order to track the person's motion accurately; to achieve this, a strong double-sided adhesive was used to fix markers to the simulation suit. In addition to having the markers securely fastened, the garment also needed to be close-fitting with minimal sliding to provide accurate motion tracking. Furthermore, the material needed to be flexible to allow a freedom of motion similar to the ideal shirtsleeves environment, applicable as the ultimate design goal for the Morphing Upper Torso. The choice of material, then, was a black spandex-like fabric for the

Figure 6. Subject wearing the simulation suit: a black, spandex-like garment with simulated scye bearings and retro-reflective markers.

simulation suit. Black Under Armour ® was chosen for this purpose. An image of the simulation suit used during testing is show in Figure 6.

D. Simulated Scye Bearings

In order to observe the (approximate) ideal location of the scye bearings of a spacesuit during human motion, it was necessary to develop simulated scye bearings for this study. As initial requirements, the scye bearing simulators needed to be lightweight and thin so as not to impede motion. However, they also needed to be sturdy enough not to deform when the arms moved. Initial testing with cardboard proved ineffectual; the material bent and folded with the motion, rather than maintaining a rigid shape. A next iteration of the design used foamcore, which was also lightweight and thin, and proved to be a sufficiently rigid material during testing. The scye bearing simulators were then formed as circular cutouts of foamcore, to which the retro-reflective markers were attached. An image of one of the scye bearing simulators is shown in Figure 4. Also, images of scye bearing simulators on a test subject can be seen in Figure 7 and Figure 8. The scye bearings were secured onto the simulation suit using Velcro® at three attachment points: on top of the shoulder, on the chest, and in the underarm region. This allowed the bearings to be taken on and off by the subject comfortably. It also allowed resizability of the bearings. Because this garment was designed to fit a number of test subjects, four sizes of shoulder bearings were made, at size increments of 0.25 inch increase in diameter between sizes. In addition to having multiple scye bearing sizes, two waist bearing simulators were developed (small and large), and two sizes of spandex suits were used. This modularity in testing apparatus allowed each subject to have a close fit of both the garment and the simulated bearings during motion tracking.

Figure 7. Subject wearing simulated scye bearings.

Figure 8. Close-up view of simulated scye bearing.

E. Motion Tasks Performed

The motions selected for this study included basic planar motion in the sagittal, coronal, and transverse planes of the body (Figure 9), as well as two non-planar motion tasks. The intent was to move the right scye bearing through the full range of motion about its local x, y, and z axes. The planar motion tasks performed in this study included: shoulder adduction/abduction, flexion/extension, and horizontal abduction/adduction. All twelve subjects performed these motions. In addition, two supplementary tasks were added to the testing routine starting with subject 4. Therefore, subjects 4 through 12 performed the planar tasks as well as two non-planar tasks: shoulder rolls and arm circles. The motion tasks are illustrated in Figure 10 through Figure 14.

The planar motion tasks were given abbreviated names during this study based on the local axis of the scye bearing about which the rotation would occur. The scye bearing axes will be defined during the data analysis section, and can be seen in Figure 16. The nomenclature for each motion task (or trial) used in this study is illustrated in Figure 10 through Figure 14.

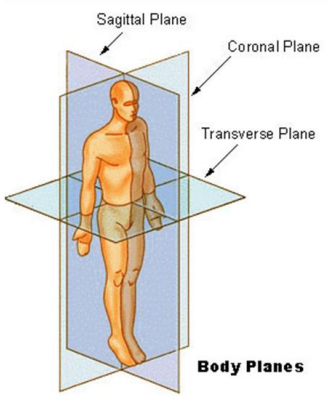

Figure 9. Body planes. *Image from Ref. 9.*

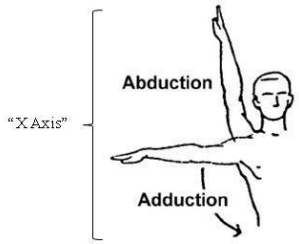

Figure 10. Shoulder abduction/ adduction. *Rotation about the local X axis of scye bearing. Trial Name: "X Axis." Image from Ref. 10.*

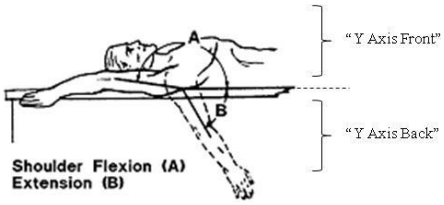

Figure 11. Shoulder flexion/extension. *Rotation about local Y axis of scye bearing. Trial Name: "Y Axis Front," in front of coronal plane. Trial Name: "Y Axis Back," behind coronal plane. Image from Ref. 11.*

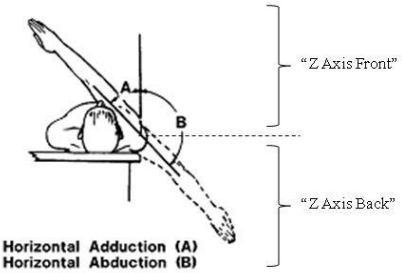

Figure 12. Shoulder horizontal abduction/ adduction. *Rotation about local Z axis of scye bearing. Trial name: "Z Axis Front," in front of coronal plane.Trial name: "Z Axis Back," behind coronal plane. Image from Ref. 11.*

F. Sample Population

The subjects who participated in this study were all volunteers in the age range of 21 to 26 years old. Data from nine male and three female subjects were included in this study. The subjects were a mixture of graduate and undergraduate students in the Aerospace Engineering Department at the University of Maryland. Information describing the subjects' characteristics is shown in Table 1. Because this study involves human subjects, approval was obtained from the Institutional Review Board (IRB) for this experiment through the University of Maryland. For confidentiality purposes, the subjects are referred to by numeric code throughout the analysis, as subjects one through twelve.

Figure 13. Shoulder rolls. *Image from Ref. 12.*

Figure 14. Arm circles. *Image from Ref. 12.*

Table 1. Characteristics of Sample Population

Subject Number	Age (years)	Height (ft)	Weight (lbs)	Gender (M/F)	Flexibility: **rarely** stretch (maybe once a month), OR **occasionally** stretch (once every week or two), OR stretch **regularly** (at least 3x per week)
1	26	5 ft 9 in	180	M	occasionally
2	22	6 ft 2.5 in	185	M	occasionally
3	21	6 ft	190	M	rarely
4	22	5 ft 9 in	140	M	rarely
5	22	6 ft 4 in	185	M	rarely
6*	-	-	-	M	-
7	22	5 ft 11 in	235	M	occasionally
8	21	5 ft 9 in	150	M	occasionally
9	22	5 ft 6 in	135	F	occasionally
10	23	5 ft 4 in	150	F	rarely
11	21	4 ft 7 in	190	M	occasionally
12	22	5 ft 3.5 in	135	F	occasionally
* Subject 6 did not fill out a questionnaire					

III. Data Analysis

Once the position data of the retro-reflective markers had been collected using the Vicon system for each trial, the data was post-processed in Vicon, exported to a trace log file (.trc), converted to an excel file, and then imported into MATLAB for analysis. Using the xyz position data of the markers, local axes were defined for each scye bearing, a rotation matrix was computed to describe the bearings' orientation in space, and Euler angles of the

bearings were calculated. In addition, marker data was also used to compute the orientation of the upper arm segment. Once the orientation angles were calculated for the scye bearing and arm, they could then be compared and heuristic correlation models developed. The range of the observed angle data was also used to describe the range-of-motion for the scye bearings, as well as the neutral pose orientation.

A. Scye Bearing Local Axes

In order to visualize the rotations of the scye bearings, it is useful to define local axes about which Euler rotations occur. For each scye bearing, the local axes are defined such that the local Y axis would point outward, away from the torso, acting along the direction of a hypothetical pressure vector if the subject were wearing a pressurized suit. The local Z axis is chosen to be in the vertical direction, relative to the person. Finally, the orientation of the local X axis is chosen in order to create orthogonality with the other two local axes. The resulting orientation of the local axes with respect to each scye bearing is shown in Figure 15 and Figure 16. Specifically, Figure 15 shows the orientation of the scye bearings when they are aligned with the base reference frame; Figure 16 shows the approximate orientation of the scye bearings relative to a person wearing a spacesuit.

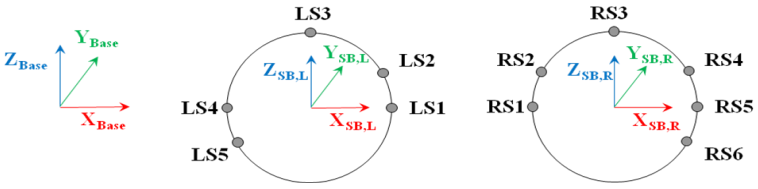

Figure 15. Scye bearing orientation when aligned with base frame. *The location of the retro-reflective markers are also shown, labeled RS1-6 for the right scye bearing, and LS1-5 for the left scye bearing. Note: In this image, the "Y" vector is pointing into the page.*

With regards to notation, the subscript "Base" is used here to refer to the coordinate base frame in which the Vicon marker position data is given. The notation LS1-5 and RS1-6 is used to label markers one through five on the left scye bearing, and markers one through six on the right scye bearing, respectively. The subscripts "SB,L" and "SB,R" are used to denote the left scye bearing and right scye bearing, respectively.

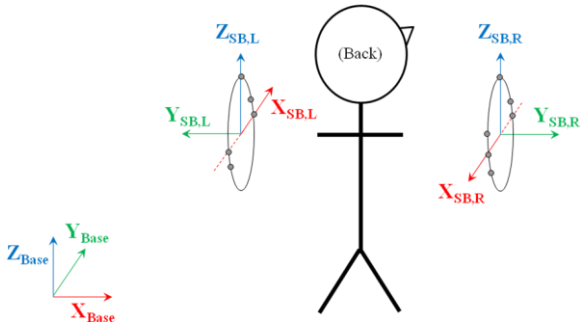

Figure 16. Scye bearing orientation on subject. *This image is shown from the rear view, such that the viewer's left and right correspond to the subject's left and right.*

In order to determine the orientation of the local axes mathematically at any point in time, it is first necessary to establish the plane of the scye bearing, using markers located on the bearing. To do this, a plane of best fit is computed using the singular value decomposition function ("svd") in MATLAB. The output of this function includes the unit normal vector to the plane of best fit. This normal vector is chosen as the local Y axis, pointing away from the torso.

Next, the local X axis is determined. During assembly of the scye bearing simulators, the location of certain markers were placed intentionally at locations diametrically opposite one another, to serve as the local X axis during data collection. These markers are denoted LS1 and LS4 for the left scye bearing, and RS1 and RS5 for the right scye bearing. The location of these markers can be seen in Figure 15. Therefore, vector addition can be used to determine the direction of the local X axis of each ring, with a mathematical correction (dot product) to ensure orthogonality with the normal to the plane of best fit, which serves as the local Y axis (labeled "$Y_{SB,R}$" in the equation below). The equation for the local X axis of the right scye bearing (denoted "$X_{SB,R}$") is shown below:

$$\overline{X_{SB,R}} = \left[\overline{RS5} - \overline{RS1}\right] - \left(\left[\overline{RS5} - \overline{RS1}\right] \bullet \frac{\overline{Y_{SB,R}}}{\left|\overline{Y_{SB,R}}\right|}\right)\left(\frac{\overline{Y_{SB,R}}}{\left|\overline{Y_{SB,R}}\right|}\right) \quad (1)$$

Once the local X and local Y axes are known, the local Z axis (or "$Z_{SB,R}$") can be computed using a cross product:

$$\overline{Z_{SB,R}} = \overline{X_{SB,R}} \times \overline{Y_{SB,R}} \quad (2)$$

B. Calculation of Scye Bearing Orientation

Following the calculation of the local axes, it is useful to normalize the vectors, converting them all to unit vectors (labeled *Xu*, *Yu*, and *Zu*, respectively). In this way, the local coordinate system is defined in terms of the base frame, which can be used to write a rotation matrix for conversions from the base frame to the local frame. Placing the components of each normalized local vector together, the rotation matrix *R* can be formed as follows:

$$R = \begin{bmatrix} Xu\,\hat{i} & Yu\,\hat{i} & Zu\,\hat{i} \\ Xu\,\hat{j} & Yu\,\hat{j} & Zu\,\hat{j} \\ Xu\,\hat{k} & Yu\,\hat{k} & Zu\,\hat{k} \end{bmatrix} \tag{3}$$

Next, it is necessary to select a desired sequence for the Euler rotations. In defining Euler rotations, the local axes must be initially aligned with the base frame[13]; subsequent rotations are performed in a specific sequence about the local axes which result in the object's final orientation. For this analysis, it is assumed that the first rotation occurs about the local Z axis, followed by a rotation about the local X axis, and completed by a rotation about the local Y axis, resulting in a 3-1-2 sequence.

This order of rotation is selected because, in order to reach the assumed neutral pose on the human body (from an initial alignment with the base frame) the scye bearings must first be rotated through an angle of +90 and -90 degrees about the local Z axis for the left and right scye bearings, respectively, as can be observed by comparing the scye bearing orientations in Figure 15 and Figure 16. Therefore, it is desirable to perform the Z rotation as the first rotation in the Euler sequence. Next, the scye bearings may be canted inward or outward relative to the torso, which would require a small rotation about the local X axis, making this the logical choice for the second rotation in the sequence. The last rotation would be performed about the local Y axis. It so happens that this is also the least interesting rotation, as it is assumed that this degree of freedom is already provided by the bearing nature of the joint, and it is therefore convenient to perform this one last. In this analysis, the variable (γ_{SB}) is used to denote rotation about the local Z axis of the scye bearing, and the variable (α_{SB}) is used to describe rotation about the local X axis of the scye bearing. The variable (β_{SB}) describes rotation about the local Y axis, but is not of interest in the analysis, as it is assumed that the scye bearing will rotate freely about the Y axis as needed, as a characteristic inherent in the bearing design.

The rotation matrix for a 3-1-2 rotation sequence can be written as follows, where *c* represents cosine, and *s* represents sine:

$$R = [R_Z][R_X][R_Y] = \begin{bmatrix} c\gamma_{SB}\,c\beta_{SB} - s\gamma_{SB}\,s\alpha_{SB}\,s\beta_{SB} & -s\gamma_{SB}\,c\alpha_{SB} & c\gamma_{SB}\,s\beta_{SB} + s\gamma_{SB}\,s\alpha_{SB}\,c\beta_{SB} \\ s\gamma_{SB}\,c\beta_{SB} + c\gamma_{SB}\,s\alpha_{SB}\,s\beta_{SB} & c\gamma_{SB}\,c\alpha_{SB} & s\gamma_{SB}\,s\beta_{SB} - c\gamma_{SB}\,s\alpha_{SB}\,c\beta_{SB} \\ -c\alpha_{SB}\,s\beta_{SB} & s\alpha_{SB} & c\alpha_{SB}\,c\beta_{SB} \end{bmatrix} \tag{4}$$

By equating the elements of Eq. (3) and Eq. (4), it is possible to calculate the Euler angles. For example, by isolating the term $s\alpha_{SB}$ in Eq. (4) and setting it equal to it is corresponding element in Eq. (3), the angle about the local X axis can be determined:

$$\begin{aligned} s\alpha_{SB} &= Yu\,\hat{k} \\ \alpha_{SB} &= \arcsin(Yu\,\hat{k}) \end{aligned} \tag{5-6}$$

Similarly, by setting up a ratio of the first two elements in the middle column of the matrix, γ_{SB} can be found:

$$\frac{-s\gamma_{SB}\, c\alpha_{SB}}{c\gamma_{SB}\, c\alpha_{SB}} = \frac{Yu\,\hat{i}}{Yu\,\hat{j}}$$

$$\tan\gamma_{SB} = -\left(\frac{Yu\,\hat{i}}{Yu\,\hat{j}}\right) \tag{7-9}$$

$$\gamma_{SB} = \arctan\left(-\frac{Yu\,\hat{i}}{Yu\,\hat{j}}\right) = -\arctan\left(\frac{Yu\,\hat{i}}{Yu\,\hat{j}}\right)$$

From this set of calculations, the Euler angles of rotation, γ_{SB} and α_{SB}, can be calculated for the scye bearing for each time step. An illustration of rotation about the local Z and local X axes is shown in Figure 17.

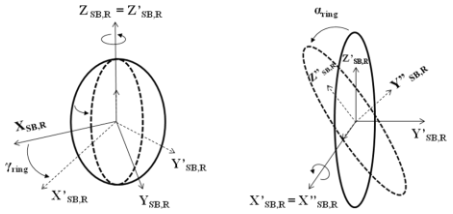

Figure 17. Visualization of rotations gamma and alpha about local axes of scye bearing.

C. Calculation of Arm Orientation

In order to investigate the possibility of a heuristic relationship between arm angle and scye bearing angle, it is necessary to calculate the orientation of the arm. In order to do this, a vector is drawn between the deltoid marker and elbow marker, representing the upper arm segment. For the right arm, this vector is called "RSE." The x, y, and z components of the RSE vector are labeled RSE(1), RSE(2), and RSE(3), respectively. In this analysis, the angles describing arm orientation are referred to as γ_{arm} and α_{arm}, and they are illustrated in Figure 18 through Figure 20.

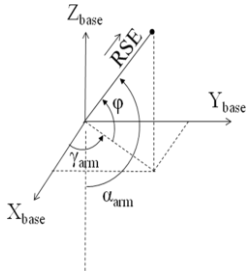

Figure 18. Illustration of alpha and gamma values for arm orientation.

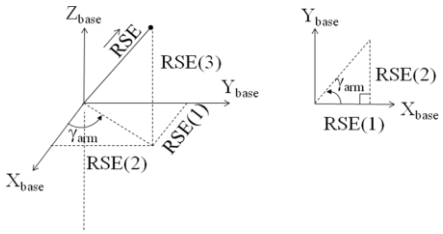

Figure 19. Illustration of gamma angle for arm.

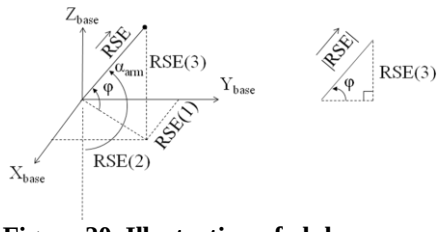

Figure 20. Illustration of alpha angle for arm.

The values of γ_{arm} and α_{arm} can be calculated using trigonometric relations between the vector components of RSE as follows:

$$\gamma_{arm} = \tan^{-1}\left(\frac{RSE(2)}{RSE(1)}\right) \tag{10}$$

$$\varphi = \sin^{-1}\left(\frac{RSE(3)}{\left|\overline{RSE}\right|}\right) \tag{11}$$

$$\alpha_{arm} = 90 + \varphi \tag{12}$$

Once the arm angles have been computed, they can be compared to the scye bearing angles in order to understand the relationship between arm motion and scye bearing motion. An illustration of the right scye bearing angles in relation to the right arm angles for $\gamma_{SB,R}$ and γ_{arm}, as well as $\alpha_{SB,R}$ and α_{arm} are provided in Figure 21 and Figure 22, respectively.

As a note, the sign convention chosen for this analysis assumes the right hand rule for determining the sign of angular rotations about the right scye bearing local axes. However, for the left scye bearing, the value of gamma does not purely follow the right hand rule; instead, a negative sign is then applied to the calculated value of gamma so that angular symmetry can be maintained, in order to provide a more intuitive measure of angular rotation. In this way, if both scye bearings were angled inward towards the body, as one is in Figure 21, it would be a positive value for gamma for both scye bearings. In other words, "pointing in" would be a positive angular rotation, and "pointing out" would be a negative rotation in gamma.

Additionally, a value of 90 degres is added to the value of gamma for the right scye bearing in order to "null" out the initial rotation from the base frame into the neutral body pose illustrated in Figure 15 and Figure 16. In this way, the values of gamma shown in the plots that follow represent the angular displacement from the at rest position, when the person's arms are at his/her sides. Similarly, a value of -90 is added to the value of gamma for the left scye bearing.

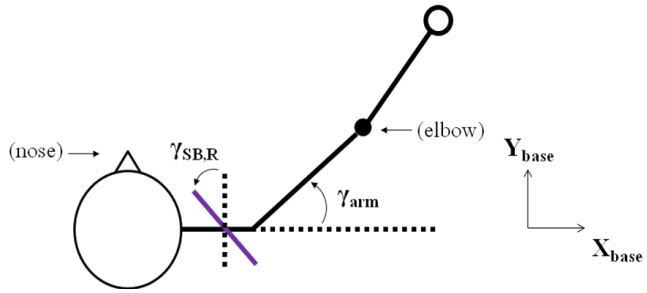

Figure 21. Sketch of gamma angles for scye bearing and arm. *The right scye bearing is shown in purple (top view).*

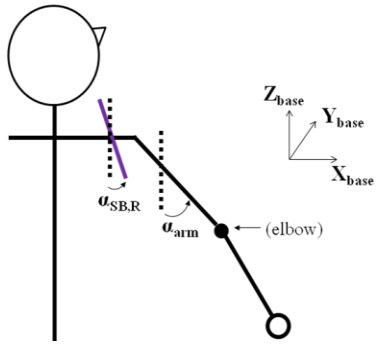

Figure 22. Sketch of alpha angles for scye bearing and arm. *The right scye bearing is shown in purple (rear view).*

IV. Results

This study investigates the behavior that a scye bearing would ideally and "naturally" have if it were provided with six degrees of freedom and could follow a human's movements without impeding them, as in near-nude body performance. It is assumed that the simulated scye bearings used in this experiment – being made of thin, lightweight material to minimize any impact they may have on human motion, and selected for close fit to follow the human arm motion as accurately as possible – that these simulated bearings would approximate the ideal position of actual scye bearings in allowing for near-nude body performance. As such, it is interesting to study their at-rest position, when the human is standing in a neutral, upright pose in Earth gravity, as it may provide insight into a preferred orientation and position for spacesuit shoulder joint design in general. For this reason, a neutral body pose analysis was performed, investigating the position and orientation of the scye bearings when at rest. Following this, the results of the ROM study are presented, describing the angular range of motion observed in the scye bearings when performing various motion tasks. Lastly, the results of the correlation investigation are presented, describing the development of heuristic models that may be used to predict scye bearing position and orientation relative to arm pose, for a specified region of motion.

D. Neutral Pose Analysis

In conducting the neutral pose analysis, it was assumed that the scye bearing simulators would settle into position after performing initial motions. Therefore, the measurement of neutral pose parameters was taken after the subject had performed at least one motion task, in order for the scye bearings to have an opportunity to "settle" into their presumed natural location. An example of a subject standing in the neutral pose is shown in Figure 23.

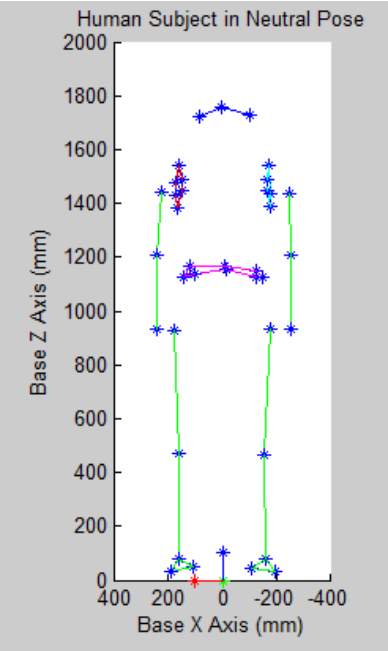

Figure 23. Example of subject in neutral pose, front view. *Image created from Vicon marker position data reconstructed in MATLAB (Subject 6).*

The first aspect investigated during the neutral pose analysis was the inter-scye bearing distance. Research questions of interest here included: could the ideal distance between scye bearing centers be predicted as a function of anthropometric dimensions, such as bideltoid breadth? The plot in Figure 24 shows the relationship observed between the subject's inter-scye bearing distance and bideltoid breadth. It appears that there is a noticeable correlation, which suggests that if a measurement is taken of distance between a subject's deltoid muscles, it may be possible to predict the "ideal" distance between scye bearing centers. This is potentially useful as a suit design metric. Before being applied widely, though, it would be beneficial to add more data points to the plot below, expanding the study to include test subjects of varying heights, stature, and musculature, which may affect the relative distance of the scye bearings.

An interesting observation regarding the plot in Figure 24 is that, of the subjects observed, a suit designer would need to account for at least 10cm of variation in scye bearing distance in order to properly design for the population used in this study. One method for providing this variation in size may be to have modular suit torsos of varying sizes to fit different people, as is done with the current NASA spacesuit, the Shuttle extravehicular mobility unit (EMU). Another option would be to have a dynamically reconfigurable suit, such as a morphing upper torso (MUT); the implication of this plot is that the MUT must be capable of at least 10cm lateral variation, and therefore must have adequate stroke length in its actuators to adjust the linkage lengths between shoulder joints accordingly.

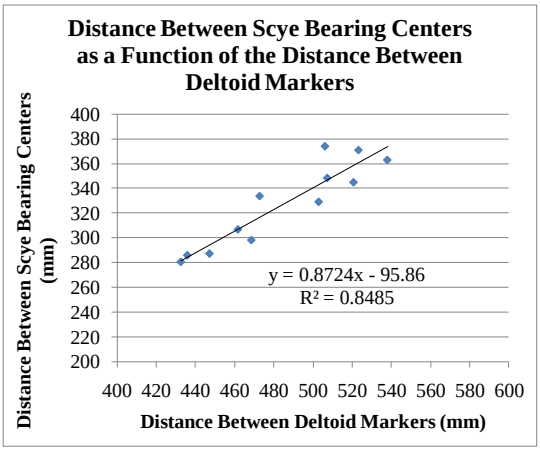

Figure 24. Plot of scye bearing distance as a function of bideltoid breadth.

After analyzing the position data of the scye bearing neutral pose, the orientation data was assessed. The research question of interest here was: is there a set of neutral angles which the scye bearing assumes consistently across subjects? If so, this could help inform future suit design decisions for scye bearing orientation. In observing the data, however, this was not found to be the case. As shown in Figure 25 and Figure 26, there is appreciable variation in the values of γ_{SB} and α_{SB} for the neutral pose. Unlike scye bearing center position, there does not appear to be a standard, common angular orientation of the scye bearings when at rest. The most that can be said for the values is that both γ_{SB} and α_{SB} appear to be "small" when the scye bearings are in their neutral pose. The average neutral pose value observed for the right scye bearing $\gamma_{SB,R}$ across all twelve subjects was 4.6 degrees, with a standard deviation of 6.2 degrees. The average neutral pose value observed for the right scye bearing $\alpha_{SB,R}$ across all subjects was 5.1 degrees, with a standard deviation of 4.6 degrees.

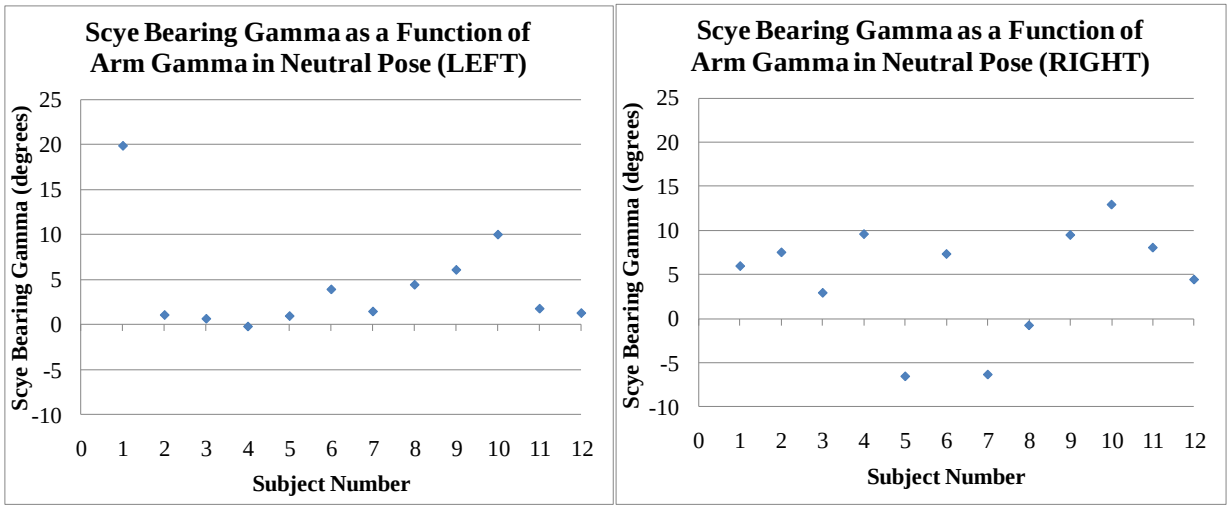

(a) **(b)**

Figure 25. Left (a) and right (b) scye bearing gamma as a function of arm gamma during neutral pose.

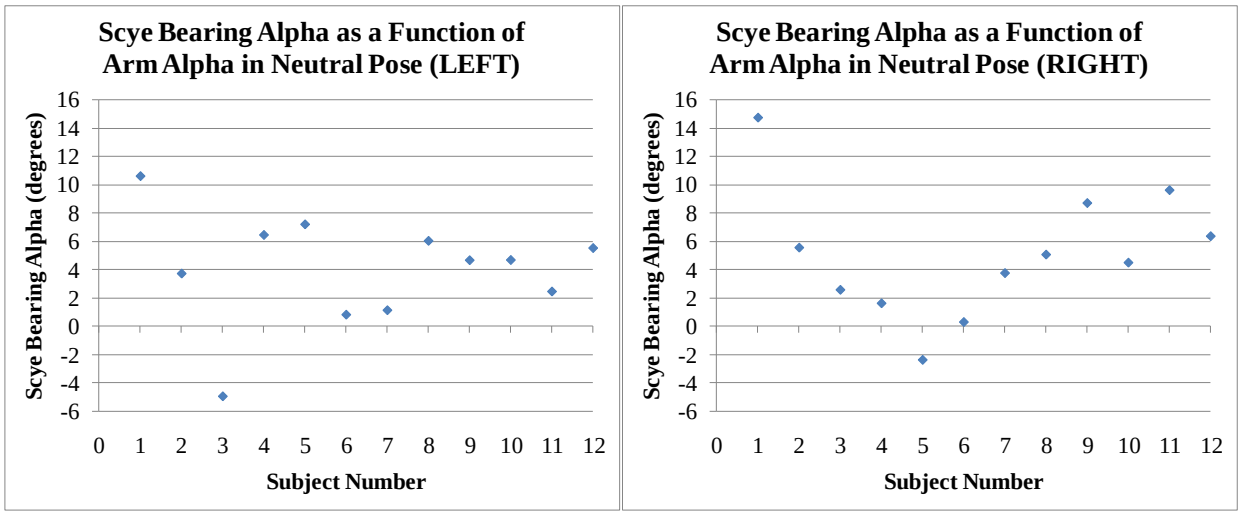

(a) **(b)**

Figure 26. Left (a) and right (b) scye bearing alpha as a function of arm alpha during neutral pose.

The next question asked was, if the scye bearings are not at a constant angle across test subjects, are they at least at a similar (i.e., symmetric) angle within the same test subject? From the plots in Figure 27 and Figure 28, it is seen that the scye bearings were not perfectly symmetric. In Table 2 and Table 3, it is seen that the average offset between left and right scye bearings for a single subject was 6.0 +/- 3.4 degrees in γ_{SB}, and 3.7 +/- 3.1 degrees in α_{SB}. This is may be due to experimental error, however, as the initial placement of the scye bearings was performed by hand, with visual inspection used to adjust the bearings for approximate symmetry. It is favorable, then, that the scye bearings were off by a comparatively little amount. Since the assumption of symmetry was made for the ROM and correlation analyses (by only analyzing the right scye bearing for those analyses), the results below are encouraging in that the scye bearings were roughly symmetric for each subject, even if not identical across subjects.

Table 2. Scye bearing gamma for left and right scye bearing of each subject.

	Comparison of Scye Bearing Gamma (degrees)		
	Left Gamma	Right Gamma	Difference
	19.8	6.0	13.9
	1.1	7.5	6.4
	0.7	2.9	2.3
	-0.2	9.6	9.8
	1.0	-6.5	7.5
	3.9	7.3	3.4
	1.5	-6.3	7.8
	4.4	-0.8	5.2
	6.1	9.5	3.4
	10.0	13.0	3.0
	1.8	8.1	6.3
	1.3	4.4	3.1
Average	4.3	4.6	6.0
Standard	5.7	6.2	3.4

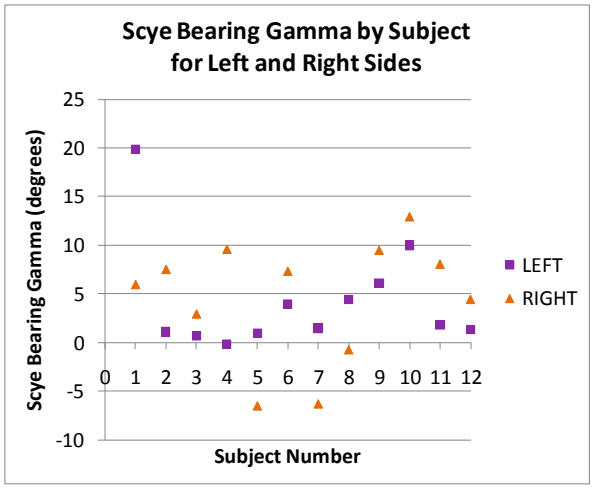

Figure 27. Comparison of scye bearing gamma for left and right scye bearing of each subject, checking for symmetry.

Table 3. Scye bearing alpha for left and right scye bearing of each subject.

	Comparison of Scye Bearing Alpha (degrees)		
	Left Alpha	Right Alpha	Difference
	10.6	14.8	4.2
	3.7	5.6	1.9
	-4.9	2.6	7.5
	6.4	1.6	4.8
	7.2	-2.3	9.5
	0.8	0.3	0.5
	1.1	3.8	2.7
	6.0	5.1	0.9
	4.7	8.7	4.1
	4.7	4.5	0.2
	2.5	9.6	7.2
	5.5	6.4	0.9
Average	4.0	5.1	3.7
Standard	3.9	4.6	3.1

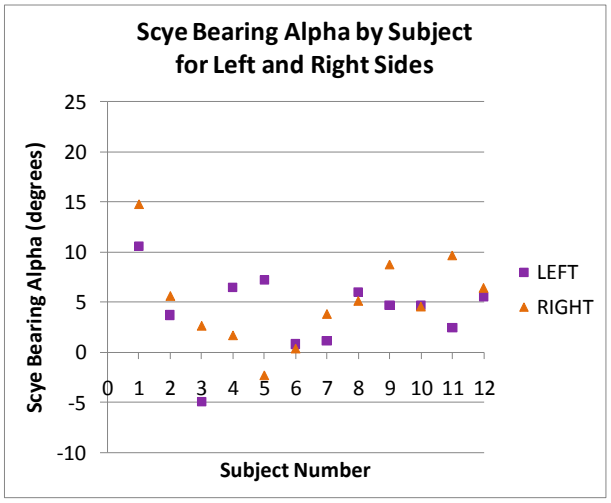

Figure 28. Comparison of scye bearing alpha for left and right bearing of each subject, checking for symmetry.

In summary, the results of the neutral pose analysis indicate that the ideal orientation of the scye bearings in the neutral pose cannot be readily predicted, at least not using the results presented in this study. However, the ideal xyz position of the scye bearing center does seem predictable based on anthropometric characteristics. In addition, the assumption of symmetry (or near-symmetry) seems to be validated for this study.

E. Range of Motion Observed

For the ROM study, the subjects performed several planar motions. Subjects 4 through 12 also performed two non-planar motions: arm circles and shoulder rolls. The ROM study shows the total range that the right scye bearing moved for each subject across all tasks he/she performed. The results of angular ROM observed for each subject are shown in Figure 29 and Figure 30 for $\gamma_{SB,R}$ and $\alpha_{SB,R}$, respectively.

As seen in Table 5, the ROM data for $\gamma_{SB,R}$ of the right scye bearing shows an average range of motion from -23 degrees to 61 degrees, with an average neutral value of 4.6 degrees. The average ROM observed for $\alpha_{SB,R}$ was approximately 1 degree through 66 degrees, with an average neutral value of 5 degrees canted inward, as seen in Table 5. The absolute maximum observed for $\alpha_{SB,R}$ during these trials was 87 degrees, exhibited by Subject 1.

However, it is useful to note that Subject 1 happened to lean during the particular trial in which the 87 degree measurement occurred, which inflates the measured value of $\alpha_{SB,R}$. Most of the subjects were instructed keep their torso facing forward and maintain their posture as level as possible, (i.e., avoid leaning and/or twisting) since the angles of arm and scye bearing both relate (either directly through trigonometric relations, or indirectly in the form of Euler angles that start aligned with the base frame) to the reference frame axes. The subjects attempted to keep the torso as level as possible during the various motion tasks; however, small variations in lean and tilt were still a source of error in this study. A recommendation for future work would be to have markers on the upper torso, perhaps placed along the sternum and spine at the height of the shoulders, which could be used to form a torso-centered reference frame. This would allow for more accurate angle measurement not affected by torso motion.

Table 4. ROM of scye bearing gamma observed for each subject.

	ROM of Scye Bearing Gamma (degrees)		
Subject #	Min	Max	Neutral Pose Value
1	-32.1	89.1	6.0
2	-20.5	55.6	7.5
3	-30.8	69.4	2.9
4	-19.8	83.2	9.6
5	-17.2	41.2	-6.5
6	-26.0	74.2	7.3
7	-40.6	37.3	-6.3
8	-20.7	52.7	-0.8
9	-16.4	42.4	9.5
10	-19.4	74.3	13.0
11	-15.4	46.5	8.1
12	-15.4	61.9	4.4
Average	-22.9	60.6	4.6
Standard Deviation	7.9	17.4	6.2
Lowest Minimum	-40.6		
Highest Maximum		89.1	

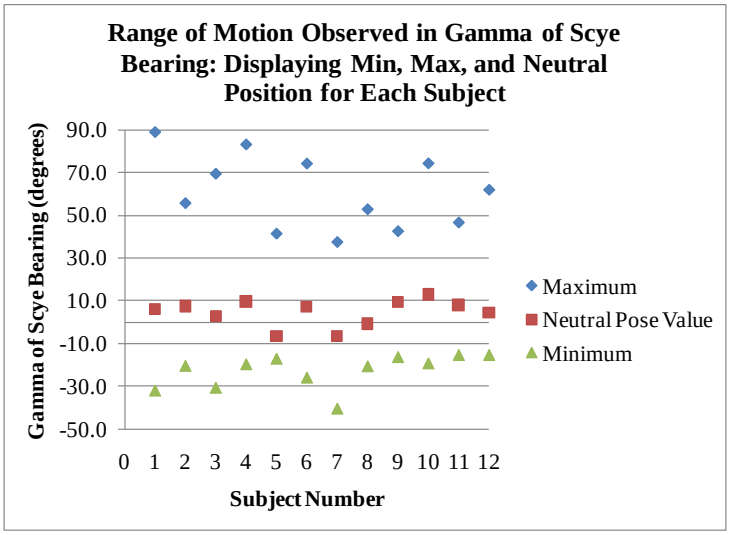

Figure 29. Plot showing the range of motion observed in scye bearing gamma for each subject.

Table 5. ROM of scye bearing alpha observed for each subject.

	ROM of Scye Bearing Alpha (degrees)		
Subject #	Min	Max	Neutral Pose Value
1	10.2	87.1	14.8
2	4.3	65.2	5.6
3	-3.2	71.4	2.6
4	0.6	72.4	1.6
5	-3.4	70.2	-2.3
6	-6.0	75.7	0.3
7	-1.9	64.7	3.8
8	1.8	57.7	5.1
9	5.7	53.2	8.7
10	-3.2	62.3	4.5
11	4.6	61.1	9.6
12	1.3	55.3	6.4
Average	0.9	66.4	5.1
Standard Deviation	4.7	9.6	4.6
Lowest Minimum	-6.0		
Highest Maximum		87.1	

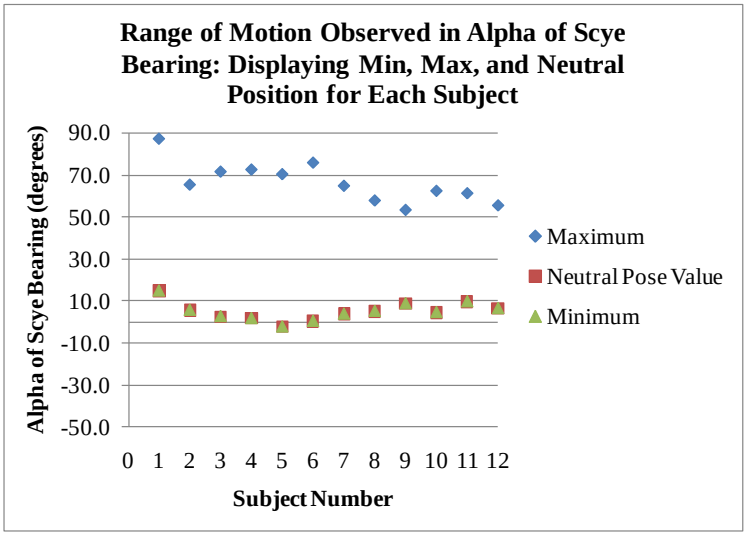

Figure 30. Plot showing the range of motion observed in scye bearing alpha for each subject.

In summary, Table 4 and Table 5 show the average range of motion needed for the right shoulder bearing of a space suit when completing these motion tasks, if the bearing were to move freely with the person as is proposed for the design of the Morphing Upper Torso. These results can be used to aid in calculating the minimum and maximum lengths needed for the prismatic linkages connecting the bearings of the torso; the subsequent requirements for linkage length would then inform design decisions for actuator stroke length for the morphing upper torso.

F. Correlation Investigation

During the initial data collection phase, it was observed that there appears to be a noticeable correlation between arm angle and scye bearing angle. Images of a few of these plots are shown below in Figure 31. If such a correlation does indeed exist, it would be useful to develop a mapping between arm pose and scye bearing pose, which could eventually could be used to dynamically control the configuration of the MUT to respond to the astronaut's motion, by predicting where the scye bearing should be for a given arm pose and then moving out of the way so as not to impede the astronaut's motion. The goal of the correlation investigation, then, was to develop a heuristic model to predict scye bearing orientation for a given arm pose. A secondary goal would be to predict the position of the scye bearing center for a given arm pose.

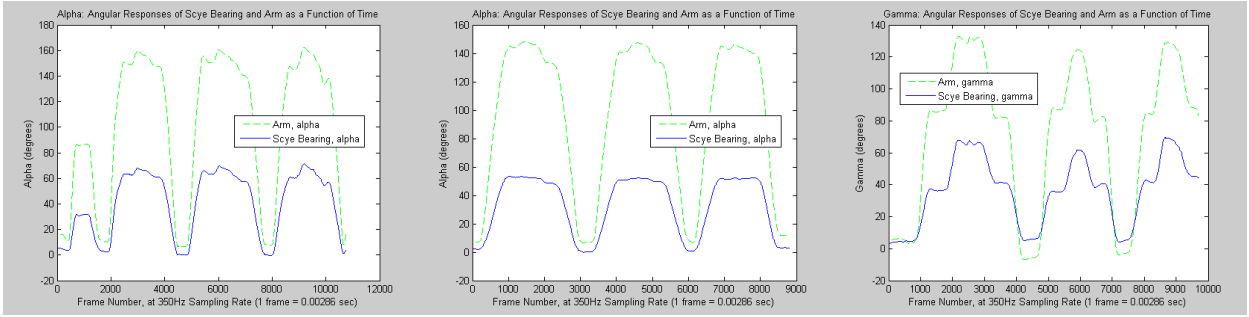

(a) **(b)** **(c)**

Figure 31. (a) Plot of arm alpha and scye bearing alpha during "X Axis" trial (Subject 3); (b) Plot of arm alpha and scye bearing alpha during "Y Axis Front" trial (Subject 3); (c) Plot of arm gamma and scye bearing gamma during "Z Axis Front" trial (Subject 3). *In each trial, subjects were asked to perform three repetitions of the motion; during several of the motion tasks, including those depicted above, there appeared to be a noticeable relationship between arm and scye bearing orientation.*

To begin the model matching investigation, the scye bearing orientation and position variables were each assumed to have linear, single-variable correlations with their analog arm variables. For instance, it was assumed that $\alpha_{SB,R}(\alpha_{arm}) = A^* \alpha_{arm} + B$. The coefficient of determination (R^2) is also presented, describing how well the model fits the data; an R^2 value closer to one indicates better fit. For this study, an R^2 value of 0.9 or greater was considered an excellent model, and a value above 0.7 an acceptable model.

The results of simple linear regression analysis for $\alpha_{SB,R}$ are shown as an example in Table 6, and the corresponding plots are shown in Figure 32. From the table and plots, it is observed that the linear model for $\alpha_{SB,R}$ has a very high coefficient of determination for certain trials, indicating that the linear model works well in certain regions of motion, but not in others. Most notably, the $\alpha_{SB,R}$ linear model has an excellent correlation value for motions during the X Axis, Y Axis Front, and Arm Circles trials, each with $R^2 > 0.95$, and with an average slope of approximately 0.4. The linear model for $\alpha_{SB,R}$ does not appear to work well for the Z Axis Front trial, or Shoulder Rolls, nor either of the motions that move the arm behind the coronal plane (Z Axis Back and Y Axis Back). (For reference, the motion trials are defined in Figure 10 through Figure 14.) Perhaps the behavior of $\alpha_{SB,R}$ is nonlinear in those regions, or perhaps it is a function of more than one variable in those regions, or perhaps no correlation exists for $\alpha_{SB,R}$ during that motion.

Table 6. Results of simple linear regression analysis for alpha, calculated for each trial using data averaged across subjects.

	Single Variable Linear Regression for Alpha: $\alpha_{SB} = A^*\alpha_{arm} + B$		
Trial	Average R^2	Average Slope, A	Average Intercept, B
X Axis	0.984	0.402	-0.00753
Y Front	0.980	0.355	0.516
Y Back	0.388	0.0129	4.04
Z Front	0.241	0.159	15.9
Z Back	0.622	0.330	3.97
Arm Circle	0.957	0.398	-3.53
Shoulder Roll	0.544	0.555	-0.0617
Average	0.674	0.316	2.98
Standard Deviation	0.305	0.178	6.27

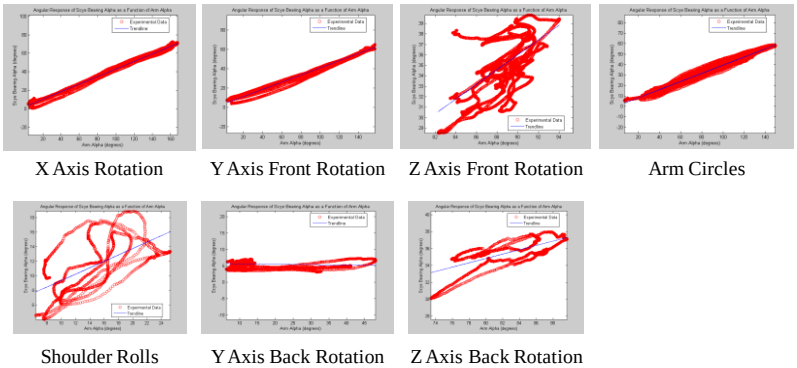

Figure 32. Example of alpha correlation trends observed for one subject during the trials (Subject 4). *Note: On each of the plots shown above, the independent variable is α_{arm}, and the dependent variable is $\alpha_{SB,R}$.*

In examining the linear regression values for $\gamma_{SB,R}$ seen in Table 7, as well as the graphical representation shown in Figure 33, it is again observed that the linear model seems to work well in certain regions, but not in others. An interesting observation here is that the linear models that exhibit a high R^2 for γ_{arm} do not necessarily have the same slope, unlike the high-correlation models for $\alpha_{SB,R,}$ which had approximately the same slope. For instance, the three best-fitting models for γ_{arm} have very different slopes (0.485, 0.37, and 0.11, respectively). The observation that the slope of gamma may be different for different regions of motion suggests that intercoupling may exist between variables. This served as motivation to attempt a multiple regression analysis.

Table 7. Results of simple linear regression analysis for gamma, calculated for each trial using data averaged across subjects.

	Single Variable Linear Regression for Gamma: $\gamma_{SB} = A*\gamma_{arm} + B$		
Trial	Average R^2	Average Slope, A	Average Intercept, B
X Axis	0.198	0.133	6.22
Y Front	0.758	0.411	-5.38
Y Back	0.842	0.110	1.65
Z Front	0.957	0.370	7.59
Z Back	0.968	0.485	6.75
Arm Circle	0.726	0.269	2.73
Shoulder Roll	0.368	0.200	3.67
Average	0.688	0.282	3.32
Standard Deviation	0.295	0.144	4.42

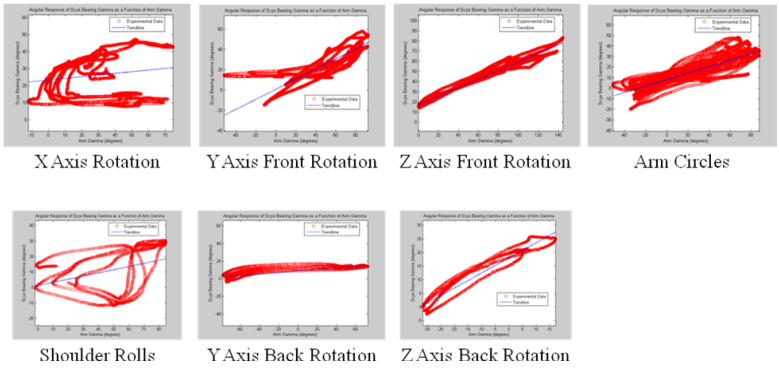

Figure 33. Example of gamma correlation trends observed for one subject during the trials (Subject 4). *Note: On each of the plots shown above, the independent variable is γ_{arm}, and the dependent variable is $\gamma_{SB,R}$.*

In developing the multiple regression analysis, it was necessary to select one of the seven trials to study in depth, in order to develop a multi-variable correlation model which would work well in that region. The "Arm Circles" trial was selected for this, as it involved a considerable range of motion through a large region of space, rather than simple planar motion, and would be more likely to reveal intercoupling effects between variables, if any existed. During the arm circles trial, each subject held their hands out to the sides, arms fully horizontally extended, then moved their arms first in small circles, then medium arm circles, followed by large arm circles. This sequence was performed first as forward arm circles, then the same pattern (small, medium, then large) was repeated for backward arm circles. Therefore, this trial captured both large and small amplitudes of motion through a sweeping range of angles mostly located in front of the coronal plane. A plot of the region swept out by the upper arm segment during one of the arm circles trials is shown in Figure 34; in the figure, the trace of the elbow tip is shown in pink, and the projection of the motion in the base xy plane (coronal plane) is shown in yellow, while the projection in the base yz plane (sagittal plane) is shown in blue.

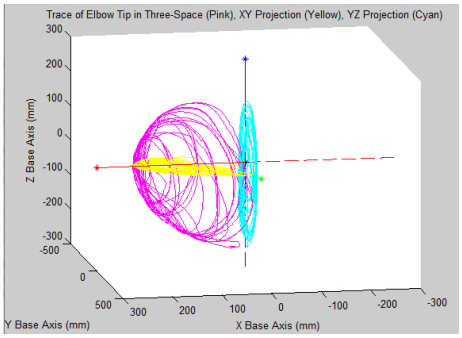

Figure 34. Plot showing the trace of elbow tip in three-space during "Arm Circles" trial (Subject 4). *Trace of elbow marker in three-space is shown in pink; projection of elbow marker motion into the xy base plane shown in yellow; projection into the base yz plane is shown in blue.*

The aim, then, was to develop heuristic models to predict the orientation and position of the right scye bearing as a function of right arm pose, if possible. The first parameter evaluated was α_{SB}. As seen in Table 8, the average R^2 was already above 0.9, so this model was deemed a valid model for this region. A plot of one subject's linear correlation model for this trial is shown in Figure 35. The average heuristic equation describing the observed behavior of α_{SB} in this region is written as:

$$\alpha_{SB} = 0.398\alpha_{arm} - 3.53 \tag{13}$$

Table 8. Parameters for heuristic model of scye bearing alpha.

	$\alpha_{SB}(\alpha_{arm})$ Correlation: Linear Approximation for Motion During Arm Circle Trial ($\alpha_{SB} = A*\alpha_{arm} + B$)		
Subject Number	R^2	A	B
4	0.975	0.388	0.467
5	0.941	0.431	-6.95
6	0.965	0.479	-8.33
7	0.971	0.415	-6.23
8	0.980	0.396	-4.38
9	0.910	0.313	2.33
10	0.962	0.390	-4.55
11	0.947	0.388	-1.99
12	0.962	0.385	-2.14
Average	0.957	0.398	-3.53
Standard Deviation	0.0217	0.0441	3.51

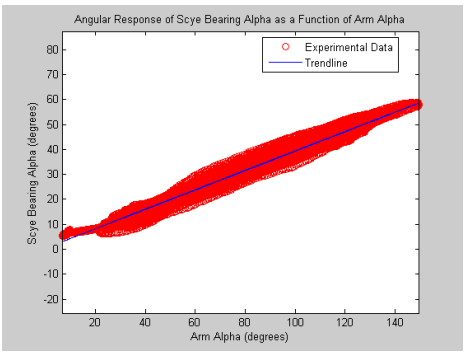

Figure 35. Example of heuristic model for alpha during "Arm Circles" trial (Subject 4).

Next, model-matching was attempted for the variable $\gamma_{SB,R}$. As with $\alpha_{SB,R}$, simple linear regression was performed first. The linear model had an average R^2 of 0.726, which is decent, but not excellent. As discussed above, it was previously observed that $\gamma_{SB,R}$ seemed to exhibit different slopes in different regions; because of this, it seems reasonable to hypothesize that it may be a function of both α_{arm} and γ_{arm}. To investigate this further, a second linear term, that of α_{arm}, was added to the linear model for $\gamma_{SB,R}$. This raised the average R^2 slightly from 0.726 to 0.776. Next, it was observed that when this model was plotted in three dimensions that the data appeared to exhibit a slight saddle-like curvature. In order to fit the curvature more closely, quadratic terms were introduced. It was found that introducing these terms raised the R^2 to 0.835. This was then declared as the heuristic model for predicting $\gamma_{SB,R}$ in this region. A set of plots showing the development of this heuristic model is shown in Figure 36. A table showing the parameters for the heuristic equation by subject is shown in Table 9. It is noted that, although the coefficients are small, they are attached to squared terms, which increases their significance. It is also noted that the standard deviation of some of the coefficients is relatively large; this may indicate that a unique equation exists for each subject. This suggests that if the morphing upper torso were a fully functioning prototype, then a calibration would have to be performed for each astronaut to determine the coefficients for his/her model prior to using the morphing upper torso. The average heuristic equation developed for $\gamma_{SB,R}$ is shown below:

$$\gamma_{SB} = -0.000169\alpha_{arm}^{\ 2} - 0.000690\gamma_{arm}^{\ 2} + 0.00262(\alpha_{arm}\gamma_{arm}) + 0.132\gamma_{arm} + 3.63 \tag{14}$$

Table 9. Parameters for heuristic model of scye bearing gamma.

		γ_{SB} Quadratic Correlation: Approximation for Motion During Arm Circle Trial ($\gamma_{SB} = A*\alpha_{arm}^2 + B*\gamma_{arm}^2 + C*\alpha_{arm}*\gamma_{arm} + D*\gamma_{arm} + E$)				
Subject Number	R^2	A	B	C	D	E
4	0.829	-0.0000248	-0.000527	0.00366	0.0563	8.85
5	0.716	0.000384	-0.000443	0.00246	0.0222	-0.726
6	0.900	-0.000488	-0.000374	0.00414	0.136	6.81
7	0.877	-0.000700	-0.000474	0.00230	0.238	-6.04
8	0.896	0.000192	-0.000973	0.00189	0.209	-2.86
9	0.671	-0.000441	-0.00158	0.00149	0.161	7.86
10	0.865	-0.000242	0.0000371	0.00277	0.0791	6.20
11	0.905	0.000198	-8.48E-05	0.000973	0.235	0.446
12	0.860	-0.000402	-0.00179	0.00388	0.0526	12.2
Average	0.835	-0.000169	-0.000690	0.00262	0.132	3.63
Standard Deviation	0.0845	0.000372	0.000635	0.00110	0.0833	6.12

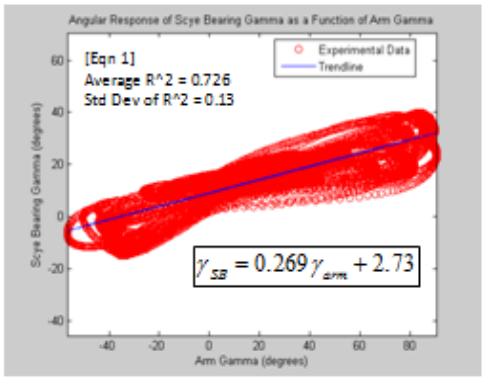

(a)

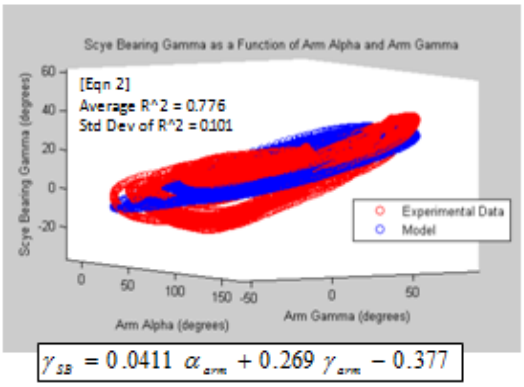

(b)

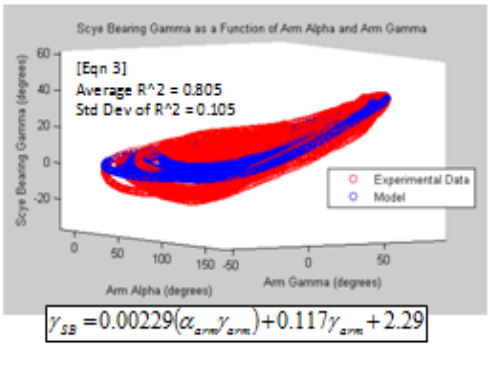

(c)

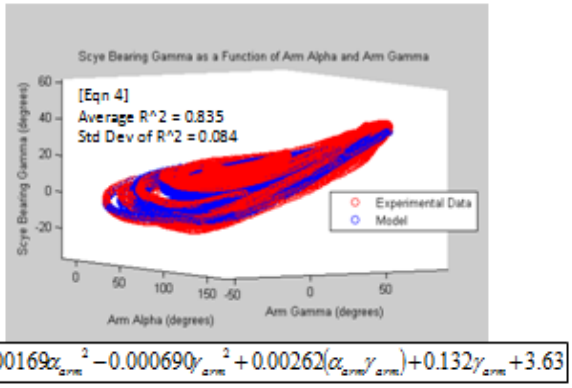

(d)

Figure 36. Model-matching process used in developing heuristic equation for scye bearing gamma (Subject 12); (a) simple linear regression, (b) multiple regression, (c) multiple regression using interaction term alpha*gamma, (d) quadratic regression. *Introducing quadratic terms in the gamma equation allowed model to conform to the saddle-like form of the observed data.*

A similar process was performed to achieve model matching for the position coordinates of the scye bearing center as a function of the Cartesian coordinates of the deltoid marker. First, the z coordinate was analyzed using simple linear regression. The results are presented in Table 10, and a plot of one subject's correlation model for this trial is shown in Figure 37. It appears that there may be some curvature at the extremes of this region. However, as the average coefficient of determination was already above 0.9, it was decided that the linear model was a close enough fit, without needing to add complexity to the model by introducing quadratic terms to account for the slight curvature. Therefore, the heuristic model for the z coordinate of the scye bearing (z_{SB}) as a function of the z coordinate of the deltoid marker ($z_{deltoid}$) is declared as:

$$z_{SB} = 0.459 * z_{deltoid} + 725 \tag{15}$$

Table 10. Parameters for heuristic model of z coordinate of scye bearing center.

	$z_{SB}(z_{deltoid})$ Correlation: Linear Approximation for Motion During Arm Circle Trial ($z_{SB} = A*z_{deltoid} + B$)		
Subject Number	R^2	A	B
4	0.911	0.581	561
5	0.923	0.437	842
6	0.913	0.494	715
7	0.884	0.457	752
8	0.946	0.487	682
9	0.879	0.438	720
10	0.866	0.448	708
11	0.940	0.373	818
12	0.890	0.417	731
Average	0.906	0.459	725
Standard Deviation	0.0280	0.0583	80.8

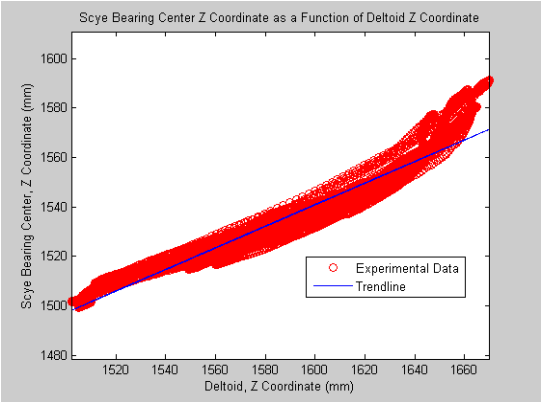

Figure 37. Example of heuristic model for z coordinate of scye bearing center during "Arm Circles" trial (Subject 5).

Next, the x coordinate correlation was examined. The simple linear regression for the x coordinate produced an R^2 of 0.4, which is comparatively low. It was observed that, as with gamma, the motion trials for which the x coordinate had exhibited a high R^2 often had a different slope; since the x coordinate appeared to have different slopes in different regions, it was concluded that the x coordinate is likely a function of more than one variable, as gamma was found to be. As a result, the x coordinate of the scye bearing center (x_{SB}) was then modeled as a function of all three position coordinates of the deltoid marker ($x_{deltoid}$, $y_{deltoid}$, and $z_{deltoid}$, respectively). The resulting model increased the average R^2 up to about 0.6, a substantial increase. It was hypothesized that perhaps the x_{SB} coordinate depended on the orientation of the arm, as well as the position of the deltoid marker. To test this theory, two additional linear terms were introduced: α_{arm} and γ_{arm}. The resulting model exhibited an average of R^2 of 0.7. Because there was not a significant amount of curvature observed in the data, there was no motivation to include quadratic terms in this model. Parameters for the heuristic are displayed by subject in Table 11. Also, a plot of one subject's correlation model for this trial is shown in Figure 38. The average heuristic equation of x_{SB} is declared as:

$$x_{SB} = 0.473 * x_{deltoid} + 0.0303 * y_{deltoid} - 0.0425 * z_{deltoid} + 0.419 * \alpha_{arm} - 0.0453 * \gamma_{arm} + 69.2 \tag{16}$$

Table 11. Parameters for heuristic model of x coordinate of scye bearing center.

		$x_{SB}(x_{deltoid}, y_{deltoid}, z_{deltoid}, \alpha_{arm}, \gamma_{arm})$ Correlation: Approximation for Motion During Arm Circle Trial $(x_{SB} = A*x_{deltoid} + B*y_{deltoid} + C*z_{deltoid} + D*\alpha_{arm} + E*\gamma_{arm} + F)$					
Subject Number	R^2	A	B	C	D	E	F
4	0.743	0.583	0.0142	-0.105	0.611	-0.0988	142
5	0.429	0.490	0.0419	0.0752	0.254	-0.0326	-62.9
6	0.832	0.463	0.0200	-0.128	0.503	0.0604	185
7	0.793	0.466	0.0791	-0.0266	0.407	-0.133	66.5
8	0.843	0.508	0.0343	0.0108	0.365	-0.0410	12.4
9	0.698	0.586	-0.00966	0.0906	0.370	-0.106	-182
10	0.827	0.391	0.0922	0.0119	0.298	-0.0190	68.3
11	0.585	0.364	-0.00845	-0.180	0.486	-0.00859	275
12	0.680	0.404	0.00926	-0.131	0.480	-0.0290	118
Average	0.714	0.473	0.0303	-0.0425	0.419	-0.0453	69.2
Standard Deviation	0.137	0.0789	0.0358	0.0973	0.111	0.0591	136

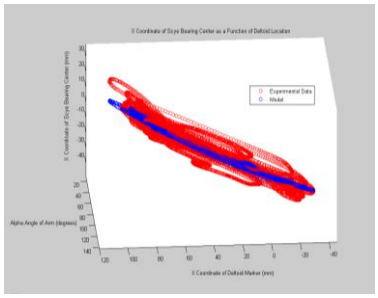

Figure 38. Example of heuristic model for x coordinate of scye bearing center during "Arm Circles" trial (Subject 12).

Lastly, a correlation for y_{SB} was developed. The initial single variable correlation provided an R^2 of 0.49. Introducing the other position variables of the deltoid marker, the coefficient of determination was increased to 0.58. Lastly, the angular terms of the arm pose were introduced and an R^2 of 0.91 was achieved. Parameters for the heuristic are displayed by subject in Table 12; an example of one subject's correlation model for this trial is shown in Figure 39. The average heuristic equation of y_{SB} was therefore declared as:

$$y_{SB} = -0.0850 * x_{deltoid} + 0.841 * y_{deltoid} - 0.0636 * z_{deltoid} + 0.344 * \alpha_{arm} - 0.507 * \gamma_{arm} + 79.3 \qquad (17)$$

Table 12. Parameters for heuristic model of y coordinate of scye bearing center.

		$y_{SB}(x_{deltoid}, y_{deltoid}, z_{deltoid}, \alpha_{arm}, \gamma_{arm})$ Correlation: Approximation for Motion During Arm Circle Trial $(y_{SB} = A*x_{deltoid} + B*y_{deltoid} + C*z_{deltoid} + D*\alpha_{arm} + E*\gamma_{arm} + F)$					
Subject Number	R^2	A	B	C	D	E	F
4	0.939	-0.0933	0.935	-0.119	0.430	-0.513	173
5	0.914	-0.0382	0.891	0.0590	0.138	-0.421	-96.3
6	0.938	-0.149	0.910	0.198	0.0463	-0.374	-287
7	0.882	-0.129	0.688	-0.00778	0.0611	-0.429	20.6
8	0.964	-0.212	0.932	-0.172	0.363	-0.602	297
9	0.933	-0.0900	0.870	-0.195	0.425	-0.412	257
10	0.910	0.00265	0.827	-0.0139	0.358	-0.397	-11.7
11	0.817	-0.140	0.781	-0.288	0.822	-0.822	385
12	0.859	0.0846	0.731	-0.0338	0.453	-0.589	-23.4
Average	0.906	-0.0850	0.841	-0.0636	0.344	-0.507	79.3
Standard Deviation	0.0462	0.0894	0.0898	0.147	0.241	0.144	215

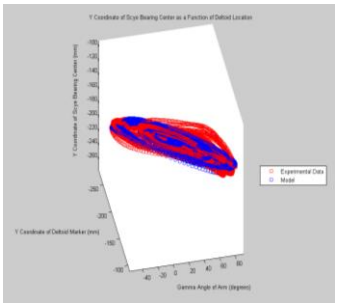

Figure 39. Example of heuristic model for y coordinate of scye bearing center during "Arm Circles" trial (Subject 12).

In summary, the initial correlation analysis revealed that simple linear regression is applicable for certain parameters over certain regions of motion, but that none of the parameters (position and orientation variables of the scye bearing) exhibited linear behavior for all motions observed. It was therefore decided to focus on developing multivariable heuristic models to characterize the behavior of the five parameters well in the most useful region observed during testing: that of the "arm circles" trial, which swept out the greatest volume and provided an opportunity to explore non-planar motion. The method of multiple regression analysis was successful in developing heuristic models for each of the five parameters describing the orientation and position of the scye bearing for a given region of motion, with an average R^2 of 0.7 or greater for the final heuristic model of each parameter. Thus, it is assumed that the motion of the scye bearing can be reasonably predicted in the region of the "arm circles" trial using these heuristic models.

It is logical to then ask whether this characterized region is indeed useful. To examine the usefulness of this characterized region, the average range of motion observed during the "arm circle" trials was compared to the NASA ROM requirements for suited motion.[11] Three of these requirements are presented below. The top row of the image indicates the NASA ROM requirement, while the bottom two rows show the analogous pose reached during the average ROM observed in subjects performing this trial. As can be seen in Figure 40, while the arm circle trials do not cover the entire range of required suit ROM, they do cover a significant portion of the suited ROM envelope, suggesting that this is indeed a useful correlation.

It is acknowledged that these heuristics are narrowly applicable to the set of subjects observed in this study. It is recommended that further testing be performed, with a broader range and number of test subjects in order to increase accuracy of the heuristics in order to make them applicable to a broader population.

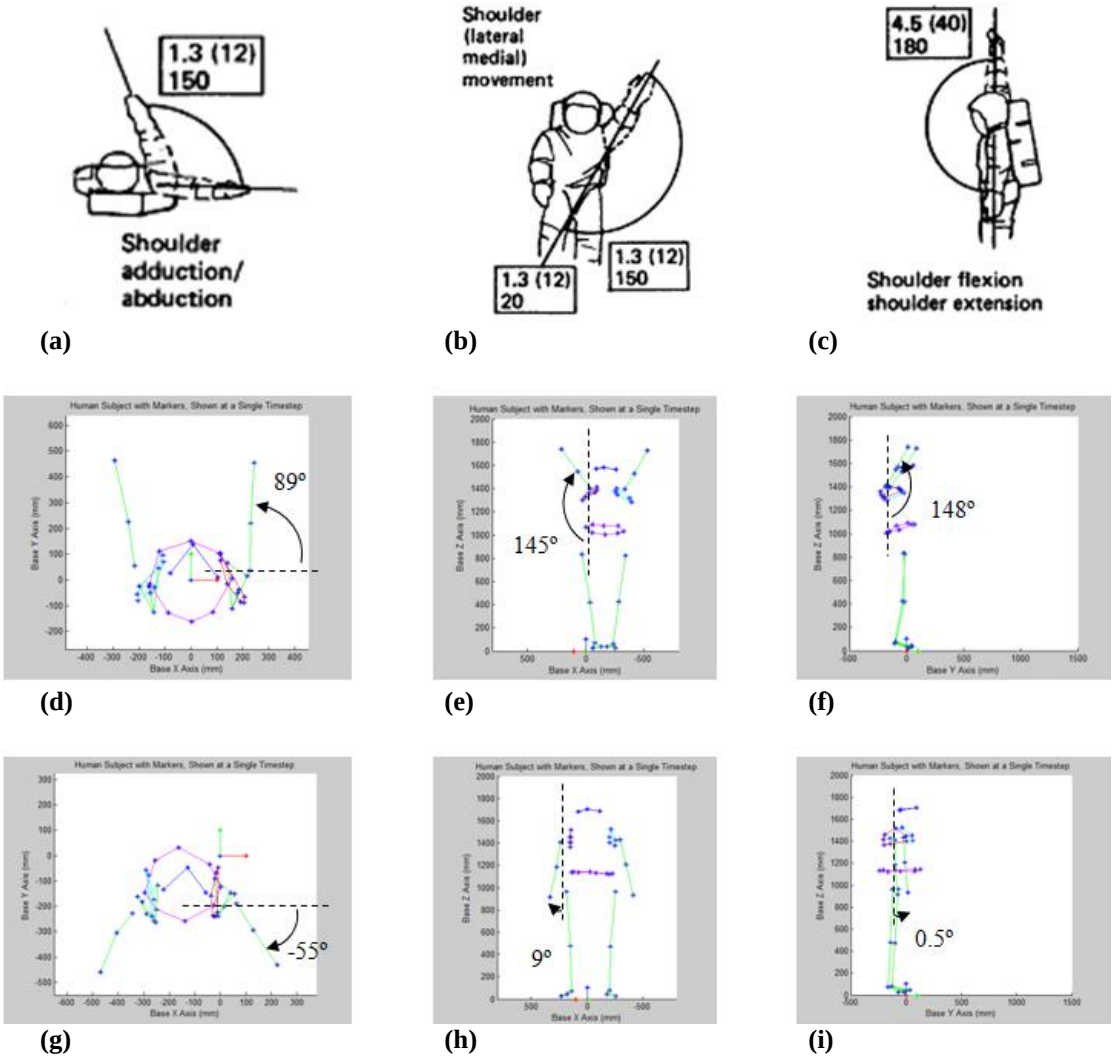

Figure 40. Illustration of suited ROM requirements compared to average ROM observed by subjects performing the "Arm Circles" trial; (a) suited shoulder horizontal adduction/abduction range, according to NASA STS suit specification[11], (b) suited shoulder abduction/adduction range, according to NASA STS suit specification[11] (c) suited shoulder flexion/extension range according to NASA STS suit specification[11]; (d) through (i) depict the minimum and maximum values of the average arm ROM observed during arm circles trial. *The trial seems to cover a significant portion of the required suit ROM, implying usefulness of the heuristic models developed.*

V. Conclusions

The Morphing Upper Torso is an innovative concept; it is an infusion of robotics and human factors to solve one of the most challenging aspects of spacesuit design: maneuverability. The research presented in this paper has endeavored to further the development of the morphing upper torso, as well as spacesuit design as a whole. The neutral pose analysis identified the appearance of a relationship between bideltoid breadth and the distance between scye bearing centers, which may be a useful metric for future suit design. In addition, it was observed that there appears to be a constant offset distance between the deltoid marker and the scye bearing center, which may serve as another useful suit metric. Following the neutral pose analysis, the results of the ROM study established an average angular range of motion for the scye bearings, which can serve as a useful reference that will inform design decisions for minimum and maximum linkage lengths, as well as actuator stroke lengths, of the morphing upper torso concept. Lastly, the correlation analysis identified that the position and orientation of the scye bearings does not appear to be a function of a single linear variable in all regions; however, a heuristic model was developed for each of the five parameters describing the pose of the scye bearing with a reasonable fit between the model and data for the region of the "arm circle" trials. This region is especially useful as it covers a large portion of the NASA required ROM for pressurized spacesuits. Therefore, this model may be useful in predicting the motion of the scye bearing throughout a large portion of the suited work envelope, which would be a crucial step towards eventually implementing a fully-functional morphing upper torso.

VI. Future Work

In future work, the results of the ROM study may be used to calculate the minimum and maximum linkage lengths, which will define requirements for actuator stroke length required for the morphing upper torso. In addition, it would be useful to continue the correlation analysis, developing a correlation model(s) that covers the entire range of NASA suited ROM specifications, thereby enabling the morphing upper torso to have the same or greater ROM as required in current pressure suits. The next step beyond would be to exceed the NASA specifications and characterize scye bearing motion the regions not included in the minimum requirements for pressure suit design, in order to achieve the goal of providing nude-body freedom of motion of the shoulder joints. Finally, the far-reaching goal is to have a suit that implements smart fabrics or other sensing techniques to determine the present position, orientation, and velocity of the astronaut's arm, can run it through the mathematical models developed to predict scye bearing motion, followed by actuation of the bearings to move with the corresponding position, orientation, and velocity needed to move out of the way so that the astronaut has complete freedom of motion within the suit, with enhanced range of motion and no exertion required to move the suit limbs of the upper torso.

The implications of a morphing space suit are intriguing, enabling enhanced motion, less fatigue, and a dramatically increased effectiveness and capability of astronauts during extra-vehicular activity. Further research in this and other areas could potentially enable a suit with those qualities. Developing the next generation of space suits is an exciting endeavor, and advancements in space suit design are likely to play a significant role in enabling humans to explore the Moon, Mars, and beyond.

Acknowledgments

Many thanks go to Dr. Shane Jacobs for his support and guidance on this project. The authors would also like to thank the personnel of the Autonomous Vehicle Laboratory for offering the use of their Vicon motion capture system and for their assistance during the data collection and post-processing efforts. Thanks are especially due to Dr. Joe Conroy, Greg Gremillion, and Evan Ulrich for offering their time and expertise with the Vicon software. Sincere appreciation also goes to Nick D'Amore for sharing his expertise on MATLAB analysis and model-matching techniques. Also, many thanks to the intrepid souls who volunteered as subjects in this study, wearing spandex and retro-reflective markers for two hours in the name of science and space exploration. Appreciation also goes to Andrew Ellsberry and Laura Meyer for their assistance during the initial development phases of the simulation suit. Thanks to all of the personnel at the Space Systems Laboratory for their assistance and advice throughout the project. Appreciation also goes to the National Science Foundation, who supported this work through a Graduate Research Fellowship to Heather Bradshaw under grant number DGE0750616.

References

[1]Harris, G. L., *The Origins and Technology of the Advanced Extravehicular Space Suit,* volume 24, AAS History Series, San Diego, CA, 2001, Chap. 1.

[2]Jacobs, S. E., "Pressure-Constrained, Reduced-DOF Interconnected Parallel Manipulators With Applications to Space Suit Design," Ph.D. Dissertation, Aerospace Engineering Dept., Univ. of Maryland, College Park, MD, 2009.

[3]Jacobs, S.E., et al., "Morphing Upper Torso: A Novel Concept in EVA Suit Design," *Proceedings of the 36th International Conference on Environmental Systems*. SAE Paper 2006-01-2142, (2006).

[4]Jacobs, S. E., Akin, D. L., "Dynamic Analysis of an Adjustable Torso Design for a Planetary Pressure Suit" ICES 2008-01-1995, *38th International Conference on Environmental Systems*, San Francisco, CA, July 2008

[5]"Motion Capture Principles," Essentials of Motion Capture for MX systems with Vicon iQ 2.0 Software. Vicon software tutorials. slides 1-4. (unpublished)

[6]Castano, L. M., Winkelmann, A. E., and Flatau, A. B., "Foot Angle Determination Using Conductive Polymer Sensors," *Proceedings of SPIE, Sensors and Smart Structures Technologies for Civil, Mechanical, and Aerospace Systems* vol. 7647, 2010.

[7]Di Capua, M., et al., "Development and Testing of Advanced Pressure Suit Technologies and Analogues for Earth-Based Simulations," *41st International Conference on Environmental Systems*, Portland, OR, July 2011 (submitted for publication)

[8]Zygote Media Group, Inc., 3D SCIENCE.COM, [Online]. Available: http://www.3dscience.com/view_image.php?imgurl=http://www.3dscience.com/img/Resources/Landing_Pages/Anatomy3.5/3D-human-anatomy.jpg&type=animframe&sizew=600&sizeh=960&title=3D%20Human%20Anatomy, 2007 [cited 5 April 2011].

[9]Anatomy Colleges.com, "Anatomical Terminology," Anatomy Schools [Online]. Available: http://www.anatomycolleges.com/Free_Course/body/terminology.html, 2011 [cited 5 April 2011].

[10]Integrated Publishing, "Figure 2-12. Range-of-motion exercises or the shoulder," www.TPUB.COM, [Online]. Available: http://www.tpub.com/content/armymedical/MD0556/MD05560061.htm, [cited 5 April 2011].

[11]Man-Systems Integration Standards, NASA-STD-3000, Technical Report Rev. B, Vol. 1, NASA [Online]. Available: http://msis.jsc.nasa.gov/Volume1.htm, July 1995 [cited 5 April 2011].

[12]Vikalp Physiotherapy Clinic, "Exercise at Work," [Online]. Available: http://vikalpphysio.in/vikalp/?page_id=547, 2011 [cited 5 April 2011].

[13]Craig, J. J., *Introduction to Robotics: Mechanics and Control*, 3rd ed., Pearson Prentice Hall, Upper Saddle River, NJ, 2005, pp. 43-45, 372.